

A second-moment closure study of rotating channel flow

By **B. E. LAUNDER, D. P. TSELEPIDAKIS AND B. A. YOUNIS**

Department of Mechanical Engineering, UMIST, Manchester, UK

(Received 6 October 1986)

The second-moment closure applied by Gibson & Launder (1978) to buoyant turbulent flows is here employed without modification to compute the effects of Coriolis forces on fully-developed flow in a rotating channel. The augmentation of turbulent transport on the pressure surface of the channel and its damping on the suction surface seem to be well captured by the computations, provided the flow near the suction surface remains turbulent. The rather striking alteration in shape of the mean velocity profile that occurs as the Rossby number is increased from 0.06 to 0.2 is shown to be explicable in terms of the modification to the intensity of the turbulent velocity fluctuations normal to the plate; for the larger value of Rossby number these fluctuations become larger than those in the flow direction causing what at low spin rates is a source of shear stress to become a sink.

1. Introduction

The fields of turbomachinery and electrical generators provide many examples of flows through rotating internal passages. At Reynolds numbers occurring in practice, the motion, in the great majority of cases, is turbulent. Within a turbine blade, for example, for a coolant passage of 1.5 mm diameter, a typical Reynolds number is 5×10^4 . Coriolis forces associated with the rotation act both directly on the mean motion and on the turbulent fluctuations. Their action on the mean flow is to induce a secondary motion while their effect on turbulence is to modify the mixing processes. Normally both effects will be present. Since secondary motions alter the turbulent stress field and modifications to the turbulence structure provide variations in the mean velocity profiles, the two effects become inextricably entwined. As a result, some of the early experimental studies have attributed to changes in turbulence structure flow developments that have more to do with the induced secondary motion.

In one case, however, the modification to the turbulence by Coriolis forces can be looked at in isolation: that of flow between infinite rotating parallel planes shown in figure 1, the mean Coriolis force in the direction normal to the planes being everywhere balanced by the pressure gradient. Measurements in rotating rectangular ducts of various aspect ratios by Launder (1965) and Moore (1967) established that, for practical purposes, the infinite-parallel-planes limit was reached for an aspect ratio of about 7:1, a configuration adopted in several later experiments. The strength of Coriolis influences is usually expressed in terms of the Rossby number which for flow in a plane channel may be taken as $\Omega D/\bar{U}$ where \bar{U} is the bulk mean velocity through the channel, D is the distance between the principal walls and Ω is the rotation rate (figure 1). The study of Johnston, Halleen & Lezius (1972) provided

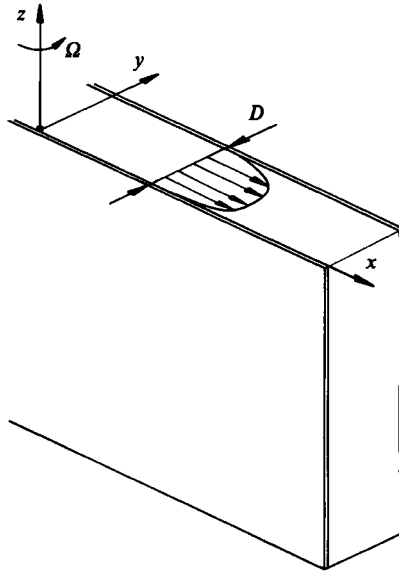


FIGURE 1. Flow configuration.

measurements over a range of Rossby numbers up to 0.21. Their photographic records of the turbulence structure indicate that on the destabilized high-pressure face of the channel, turbulent eddies aggregated into large-scale Görtler-type vortices for Rossby numbers greater than 0.15 while, at the low Reynolds numbers of their experiments, turbulent mixing was virtually annihilated on the low-pressure face. Even for Rossby numbers as low as 0.01 measurements of mean velocity and wall friction (Launder 1965; Moore 1967; Johnston *et al.* 1972) still indicate a significant alteration in the turbulence structure. While Koyama & Ohuchi (1985) report streamwise turbulence intensities in developing flow in rotating passages, no experimental data of the turbulent velocity field appear to have been reported for fully-developed rotating channel flow. Kim (1983), however, has performed a large-eddy simulation for a moderate Rossby number (0.068) which provides an indication of how rotation modifies the directional turbulence intensities. Very recently Miyake & Kajishima (1986) have reported large-eddy simulations up to Rossby numbers of 0.2. While the rather coarse grid employed may limit the value of these results as a formal database, they show interesting developments in the partitioning of the normal stresses. At the highest Rossby numbers, over a not inconsiderable region of their channel, the turbulence intensity normal to the wall was larger than the corresponding streamwise fluctuations, quite the reverse of that found in a stationary channel.

Because flows in rotating passages arise in expensive, high-technology equipment, there is considerable interest in being able to calculate their development reliably. Eddy viscosity models of turbulent transport developed for non-rotating systems do not extrapolate well to rotating conditions. In such schemes changes in effective transport coefficients are closely linked with changes in the turbulent kinetic energy – yet, there is no direct effect of rotation on the turbulence energy budget. Workers adopting this approach have usually tried to account for Coriolis influences on the turbulence by modifying the turbulent lengthscale or, equivalently, adding rotation-dependent terms to a closed-form transport equation for ϵ , the turbulence-

energy dissipation rate. The work of Howard, Patankar & Bordyniuk (1980) provides a good example of this approach and references to earlier contributions of the same type.

If one considers the dynamic equations for the individual normal stresses, rotational influences become plain: a term $4\overline{uv}\Omega$ appears as a source (or sink, depending on the sign of \overline{uv}) in the budget for the mean square streamwise turbulent velocity $\overline{u^2}$, while a sink (source) of the same magnitude appears in the corresponding equation for the velocity fluctuations normal to the wall $\overline{v^2}$. Now, turbulent momentum transport rates are far more sensitive to changes in fluctuations normal to the channel wall than to those in the mean flow direction since that is the direction of inhomogeneity in mean velocity. Thus, if $\overline{v^2}$ is damped, so too will be the rate of mean momentum transfer irrespective of any increase in the streamwise turbulence intensity. The above feature of rotating flows suggests that a second-moment closure should be a promising route to adopt, that is to say one based on a closed-form version of the transport equations for the turbulent stress components. While models of this type have been rather successful in accounting for the effects that streamline curvature and buoyancy have on turbulence, there probably remains a degree of scepticism as to whether such schemes will predict transport rates correctly when markedly different large-eddy structures are created. Pouagare & Lakshminarayana (1983) have in fact started from a second-moment closure to guide them in developing an eddy viscosity model with a diffusion coefficient dependent on rotation rate. While the trends of the data were captured, both the mathematical simplifications made and the non-negligible differences between computation and experiment left the question of extrapolation unresolved. The same remarks may be made of the full second-moment closure study of Masuda, Koyama & Ariga (1983) who employed the quasi-isotropic pressure-strain model (Launder, Reece & Rodi 1975), that is applicable only to free shear flows. The decisive effect of a rigid boundary on pressure fluctuations, particularly in the presence of force fields, may be inferred from the quite different effects of gravitational forces on the turbulence structure in free shear flows and in the near-ground region of the earth's boundary layer, Gibson & Launder (1978).

The aim of the present study has thus been to test directly whether a full second-moment closure developed for non-rotating simple wall flows does or does not reproduce the trends of the available experimental data with at least sufficient fidelity for engineering computations.

2. The physical and mathematical model

The mean momentum equation describing the fully developed uniform-property flow through a parallel-walled channel rotating at angular velocity Ω may be written:

$$0 = -\frac{1}{\rho} \frac{dP^*}{dx} - \frac{d}{dy} \overline{uv} + \nu \frac{d^2U}{dy^2}. \quad (1)$$

Here x and y are respectively the flow direction and the direction normal to the planes in a Cartesian frame rotating about the z -axis with the same angular velocity as the channel. P^* is the 'reduced' static pressure and dP^*/dx is a constant whose magnitude determines the mass flow rate between the planes. Formally, therefore, the mean momentum equation is identical to that for the non-rotating case. Over the region of flow considered, the viscous diffusion term in (1) is of only minor significance and the equation thus imposes the constraint that the turbulent shear

stress \overline{uv} varies (very nearly) linearly across the channel. Thus, paradoxically, the mean momentum equation fixes the Reynolds shear stress \overline{uv} while the equation for \overline{uv} can be regarded as the vehicle for determining the mean velocity profile, $U(y)$.

Of course, in second-moment closure the shear stress cannot be found independently of the other Reynolds-stress components. Each is described by the following equation written for compactness in Cartesian tensor notation:

$$\frac{D\overline{u_i u_j}}{Dt} = P_{ij} + G_{ij} + d_{ij}^v + d_{ij} + \Phi_{ij} - \epsilon_{ij}, \quad (2)$$

where

$$P_{ij} \equiv - \left\{ \overline{u_i u_k} \frac{\partial U_j}{\partial x_k} + \overline{u_j u_k} \frac{\partial U_i}{\partial x_k} \right\}, \quad G_{ij} \equiv -2\Omega_k \{ \overline{u_j u_m} \epsilon_{ikm} + \overline{u_i u_m} \epsilon_{jkm} \},$$

$$d_{ij}^v \equiv \nu \frac{\partial^2 \overline{u_i u_j}}{\partial x_k^2},$$

$$\Phi_{ij} \equiv \frac{p}{\rho} \left(\frac{\partial u_i}{\partial x_j} + \frac{\partial u_j}{\partial x_i} \right),$$

$$\epsilon_{ij} \equiv 2\nu \frac{\partial u_i}{\partial x_k} \frac{\partial u_j}{\partial x_k},$$

$$d_{ij} \equiv - \frac{\partial}{\partial x_k} \left(\overline{u_i u_j u_k} + \frac{p}{\rho} \overline{u_i} \delta_{jk} + \frac{p}{\rho} \overline{u_j} \delta_{ik} \right).$$

The quantities P_{ij} and G_{ij} , the stress generation associated with shear and rotation (like the very minor contribution from viscous diffusion, d_{ij}^v) need no approximation comprising only Reynolds-stress components and mean field quantities.

Since G_{kk} vanishes, there is no direct turbulence energy created by the rotation. If we take Ω_k as $(0, 0, \Omega)$, the positive y - (x_2)-direction points in the direction that the duct is moving (figure 1). Thus, for a mean flow that is radially outward, $\partial U/\partial y$ is positive (and hence \overline{uv} negative) near the pressure face. The rotational term in the $\overline{v^2}$ equation, $-4\Omega\overline{uv}$, is thus positive, producing enhanced turbulent transport as discussed in §1. The same rotational term with opposite sign appears in the $\overline{u^2}$ equation, while in the shear-stress equation the rotational term is $-2\Omega(\overline{u^2} - \overline{v^2})$. In the usual thin-shear-flow situation $\overline{u^2}$ exceeds $\overline{v^2}$, so on the pressure side of the channel where $\partial U/\partial y$ is positive, the rotational and shear-generation terms are of the same sign while on the 'suction' side they oppose one another.

Surrogate models have to be provided for the remaining processes in (2) before it can be used to determine the turbulent stress field. The turbulent stress diffusion process (d_{ij}) is approximated by the generalized-gradient-diffusion hypothesis of Daly & Harlow (1970) while local isotropy is assumed for the dissipative correlations (ϵ_{ij}). Thus:

$$d_{ij} = \frac{\partial}{\partial x_l} \left(c_s \frac{k}{\epsilon} \overline{u_l u_k} \frac{\partial \overline{u_i u_j}}{\partial x_k} \right), \quad (3)$$

$$\epsilon_{ij} = \frac{2}{3} \delta_{ij} \epsilon, \quad (4)$$

where k and ϵ are the turbulent kinetic energy and its dissipation rate.

The model for the pressure-strain process is broadly taken over from Gibson & Launder (1978). The term is made up of contributions as follows:

$$\Phi_{ij} = \Phi_{ij1} + \Phi_{ij2} + \Phi_{ij3} + \Phi_{ijw},$$

the separate elements being associated respectively with purely turbulence interactions, mean strain, rotation and, finally, pressure reflections from the wall. Rotta's (1951) linear return-to-isotropy model is retained for the first of these:

$$\Phi_{ij1} = -c_1 \frac{\epsilon}{k} (\overline{u_i u_j} - \frac{1}{3} \delta_{ij} \overline{u_k u_k}), \quad (5)$$

while the analogous isotropization-of-production (IP) model is used for both the mean-strain and rotational parts of Φ_{ij} . Thus, for the mean-strain part:

$$\Phi_{ij2} = -c_2 (P_{ij} - \frac{1}{3} \delta_{ij} P_{kk}). \quad (6)$$

A little care is needed in extrapolating this idea to the case of rotating flow, essentially because the substantial derivative $D\overline{u_i u_j}/Dt$ is not, as it stands, materially invariant. A frame-indifferent convective derivative may, however, be obtained in several ways. Two that suffice for present purposes are either to add P_{ij} to each side of (2) (Eringen 1962):

$$C'_{ij} \equiv \frac{D\overline{u_i u_j}}{Dt} + P_{ij} = 2P_{ij} + G_{ij} \dots,$$

or to assign half the rotation 'generation' to the convection term (Takhar & Thomas 1985):

$$C''_{ij} \equiv \left(\frac{D\overline{u_i u_j}}{Dt} - \frac{1}{2} G_{ij} \right) = P_{ij} + \frac{1}{2} G_{ij} + \dots$$

Either approach suggests that in applying the isotropization-of-production idea to rotating systems the effective generation associated with rotation is only half as great relative to shear generation as indicated by (2). (The same conclusion is reached from considering the Poisson equation for fluctuating pressure, e.g. Cousteix & Aupoix 1981; Bertoglio 1982. The former reference obtained the rotating-flow version of the 'quasi-isotropic' model of ϕ_{ij2} , a representation which, while emerging from formal analysis, is less successful in practice than the simpler, intuitive IP model used here). One must of course adopt the same coefficient in the mean-strain and rotational parts of Φ_{ij} ,† so we infer that

$$\Phi_{ij2} + \Phi_{ij3} = -c_2 (P_{ij} + \frac{1}{2} G_{ij} - \frac{1}{3} \delta_{ij} P_{kk}), \quad (7)$$

since $G_{kk} = 0$. The value 0.6 is retained for c_2 since this satisfies Crowe's (1968) exact result:

$$\Phi_{ij2} = 0.4k \left(\frac{\partial U_i}{\partial x_j} + \frac{\partial U_j}{\partial x_i} \right),$$

in the limit of isotropic turbulence.

Finally, following Shir (1973) and Gibson & Launder (1978), pressure reflections from the walls of the channel are modelled as:

$$\begin{aligned} \Phi_{ijw} = & \left\{ c_{1w} \frac{\epsilon}{k} [\overline{u_k u_m} n_k n_m \delta_{ij} - \frac{3}{2} \overline{u_k u_i} n_k n_j - \frac{3}{2} \overline{u_k u_j} n_k n_i] \right. \\ & + c_{2w} [(\Phi_{km2} + \Phi_{km3}) n_k n_m \delta_{ij} - \frac{3}{2} (\Phi_{ik2} + \Phi_{ik3}) n_k n_j \\ & \left. - \frac{3}{2} (\Phi_{jk2} + \Phi_{jk3}) n_k n_i] \right\} f \left(\frac{k^{\frac{3}{2}}}{\epsilon n_q r_q} \right), \quad (8) \end{aligned}$$

† Otherwise, in computing a flow like an axisymmetric swirling jet, the computed behaviour would differ according to the rate of rotation of the axes.

c_1	c_2	c_{1w}	c_{2w}	c_s	$c_{\epsilon 1}$	$c_{\epsilon 2}$	c_ϵ
1.8	0.6	0.5	0.3	0.22	1.45	1.90	0.18

TABLE 1. Values of empirical coefficients

where n denotes the vector normal to the wall. As in most earlier studies the wall proximity function f is interpreted as the summation of effects from both walls of the channel:

$$f(\cdot) \propto \frac{k^{\frac{3}{2}}}{\epsilon} \left(\frac{1}{y} + \frac{1}{D-y} \right), \quad (9)$$

the constant coefficient being chosen so that f equals unity in the vicinity of the wall.

The energy dissipation rate, ϵ , appearing in various terms above is obtained from its own transport equation:

$$\frac{D\epsilon}{Dt} = c_{\epsilon 1} \frac{\epsilon}{k} \frac{1}{2} P_{kk} - c_{\epsilon 2} \frac{\epsilon^2}{k} + c_\epsilon \frac{\partial}{\partial x_k} \left(\frac{k}{\epsilon} u_k u_l \frac{\partial \epsilon}{\partial x_l} \right). \quad (10)$$

Equation (10) is again a widely employed form that has been in use for some fifteen years (Hanjalić & Launder 1972). The standard values of the empirical coefficients adopted for the calculations are listed in table 1; in no case have they been tuned to secure better agreement with experiment.

The numerical computations have been made with an adapted version of *PASSABLE* (Leschziner 1982), a general-purpose finite-volume solver for strings of coupled two-dimensional parabolic differential equations. As only the fully-developed solution was under consideration, however, the streamwise convection terms were dropped and, in place of forward-marching, in-step iterations were made until the difference equations were accurately satisfied.

The model for the Reynolds stresses described in the preceding paragraphs is not applicable to the semi-viscous sublayers immediately adjacent to the walls. Boundary conditions on both sides of the channel are therefore applied far enough from the surface for the near-wall node to lie in the fully turbulent region. There the relation between the near-wall velocity and local shear stress is fixed from the usual logarithmic law:

$$\frac{U}{U_\tau} = \frac{1}{\kappa} \ln y^+ + c,$$

where U_τ is the friction velocity at the wall in question, y^+ is the distance from the nearby wall multiplied by U_τ/ν and constants κ and c take the value 0.41 and 5.0 recommended by Coles (1956). The dimensionless stress ratios at the near-wall nodes were fixed by assuming a constant stress layer while ϵ was obtained from a quadratic equation that results from assuming a dependence inversely proportional to wall distance.

In addition to the near-wall boundary points, 47 interior nodes were employed in the solutions, somewhat concentrated towards the walls where gradients of the dependent values (in particular of ϵ and U) are steepest.

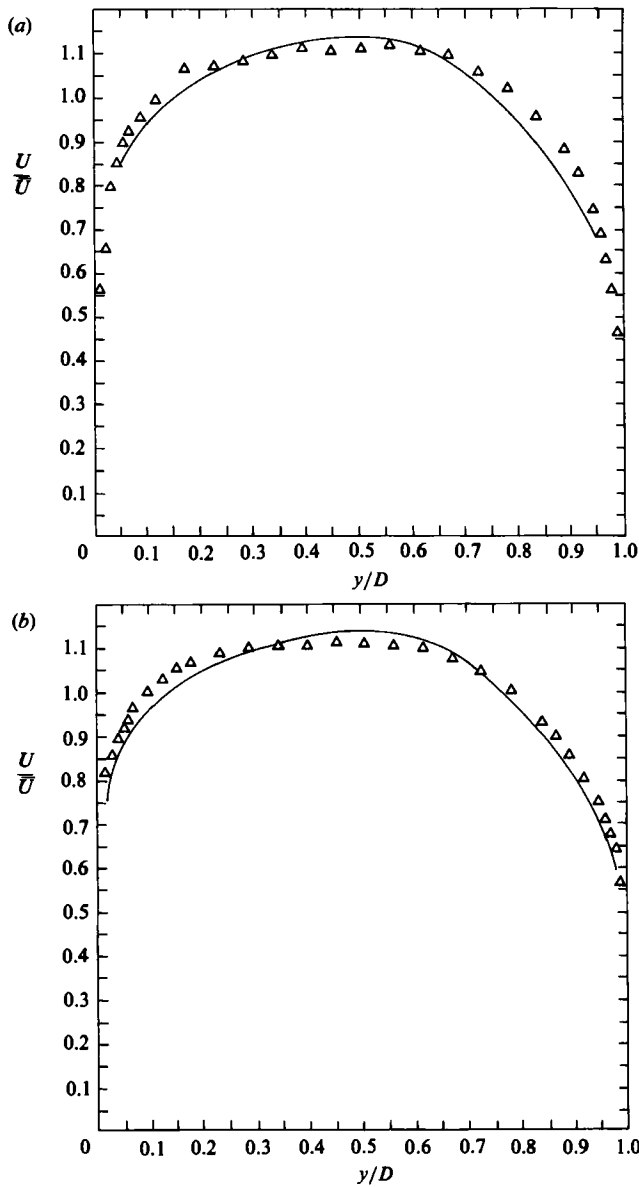


FIGURE 2(a, b). For caption see facing page.

3. Presentation and discussion of the results

Figure 2 compares the computed mean velocity distribution between the planes with the experimental data of Johnston *et al.* (1972) for two values of Rossby number, $Ro (\equiv \Omega D / \bar{U})$ and two Reynolds numbers, $Re (\equiv \bar{U} D / \nu)$, \bar{U} being the bulk mean velocity. In comparison with non-rotating channel flow, the profile on the unstable side initially steepens near the wall but exhibits a more uniform level further from the wall than for zero rotation. There are less pronounced changes on the stable side of the channel, though the maximum velocity position shifts to the stable side of the geometric symmetry plane. An increasingly asymmetric appearance develops as the

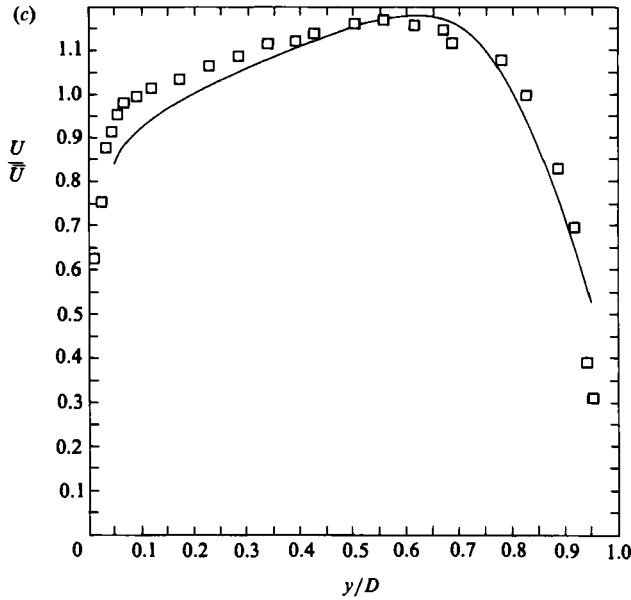


FIGURE 2. Mean velocity distribution across the channel. Symbols, experiment Johnston *et al.* (1972); line, present computations. (a) $Re = 11\,500$, $Ro = 0.068$. (b) $Re = 35\,000$, $Ro = 0.068$. (c) $Re = 11\,500$, $Ro = 0.21$.

rotation rate increases. The rather flatter measured profile in the central region for $Re = 35\,000$ may (as Johnston *et al.* suggest) be partly due to their flow not having reached full development. Kim's large-eddy simulation produces a profile shape closer to the present computations than the experimental data. At the higher rotation number, 0.21, there is a rather different velocity variation over the 'unstable' side of the velocity maximum, the region of steep slope near the wall giving way to a gentle linear increase in velocity but with a slope greater than at lower Rossby numbers. The reason for this different shape of velocity distribution will emerge later when the turbulence intensity profiles are discussed. Overall, the departures of the mean velocity profiles from symmetry are reasonably well captured by the computations. (It is worth underlining that an eddy-viscosity model developed for non-rotating flows would exhibit complete symmetry at all rotational speeds.)

When the velocity distribution is viewed in wall coordinates, figure 3, it is evident that on the stable side of the channel the 'wake' component of the profile is enhanced while on the unstable side it is completely eliminated. The two computational results on this figure were made for the dynamic conditions of Kim's (1983) large-eddy simulation and for conditions intermediate between two of the tests of Johnston *et al.* (1972). There is generally satisfactorily close agreement among the experimental data, Kim's results and the present second-moment computations.

As the Rossby number is raised, the computed position of zero shear stress also shifts towards the suction surface, only rather more quickly than the peak velocity location. Thus, just as in flow through a channel with one smooth and one rough wall, the position of zero shear stress is located nearer than the point of maximum velocity to the wall with the lower shear stress. The experiments of Johnston *et al.* (1972) are qualitatively in accord with this result, though accurate experimental values are hard to determine as the velocity profile is so flat in the vicinity of its maximum.

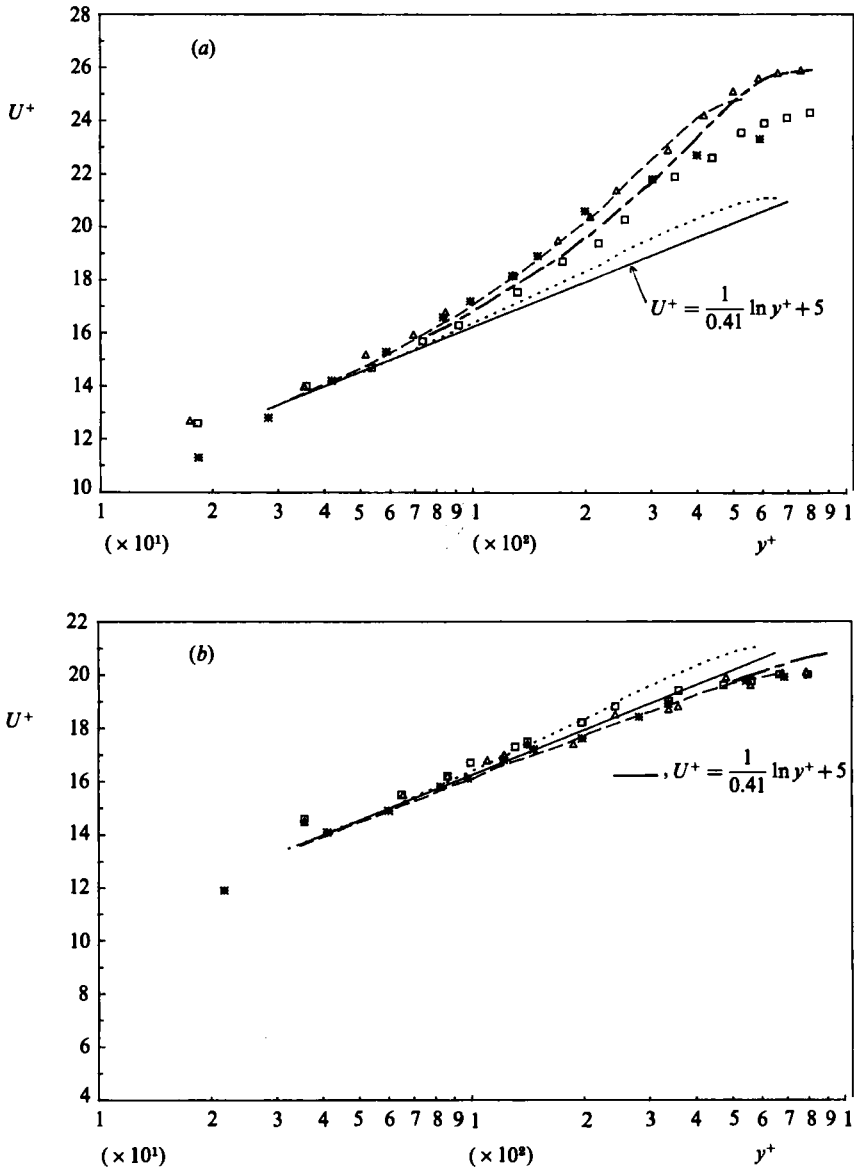


FIGURE 3. Mean velocity profile in wall-law coordinates. (a) Stable side of the channel. (b) Unstable side of the channel. Experiments by Johnston *et al.* (1972): \triangle , $Re = 34400$, $Ro = 0.083$; \square , $Re = 33300$, $Ro = 0.058$. Large-eddy simulation by Kim (1983): $*$, $Re = 24600$, $Ro = 0.068$. Present computations: ---, $Re = 24600$, $Ro = 0.068$; —, $Re = 35000$, $Ro = 0.068$; \cdots , $Re = 24600$, $Ro = 0$.

The r.m.s. turbulent velocities normal to the wall and in the stream direction are compared with those generated by Kim's simulation in figure 4. (The fluctuations in the z -direction are almost unmodified by the rotation at this value of Ro and are therefore omitted for clarity.) The changes due to rotation are mainly in the directions one would infer from the sign of the Coriolis terms in the $\overline{u^2}$ and $\overline{v^2}$ equations. Near the unstable wall an augmentation of v' ($\equiv (\overline{v^2})^{1/2}$) occurs with a reduction in u' ; the reverse effects are seen on v' on the stable side, though u' there is little affected by

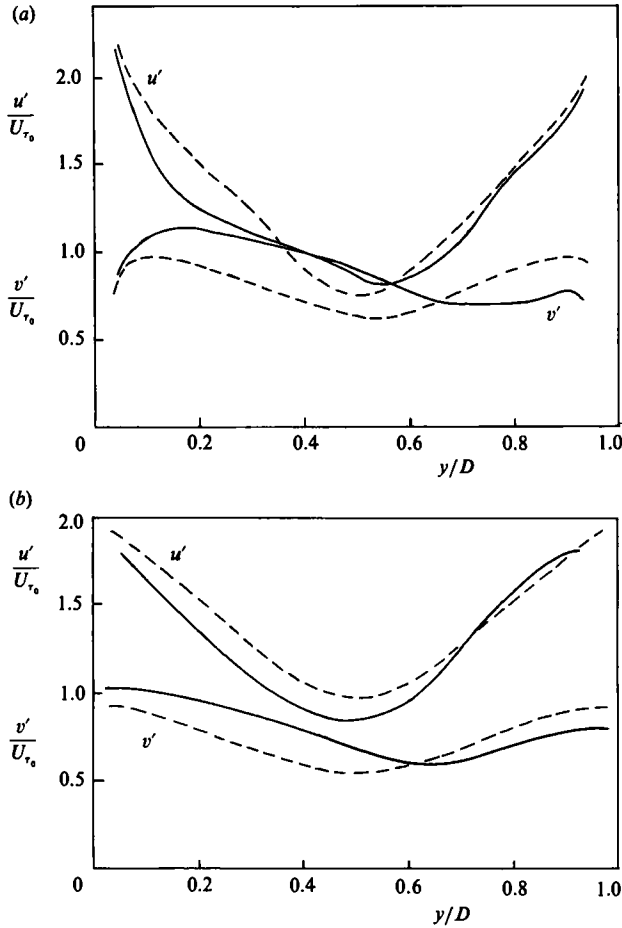


FIGURE 4. Profiles of fluctuating velocities normalized by mean friction velocity for non-rotating flow at the same Reynolds number. (a) Large-eddy simulation by Kim (1983): —, $Re = 24600$, $Ro = 0.068$; ---, $Re = 24600$, $Ro = 0$. (b) Present computations: —, $Re = 24600$, $Ro = 0.068$; ---, $Re = 24600$, $Ro = 0$.

rotation. Qualitatively the present computations reproduce all these features, though in the centre of the channel certain discrepancies are evident. Kim's computations indicate that in this region v' becomes as large as u' , a result not reproduced by our calculations which, in any event, give a too strongly anisotropic stress in the centre of the channel even for zero rotation. This (not very important) defect is due to the wall damping function f not decreasing rapidly enough with wall distance. † Bardina, Ferziger & Reynolds (1983; see also Bardina, Ferziger & Reynolds 1985) have pointed out that the dissipation-rate transport equation needs to be made sensitive to rotation if the decay of turbulence behind a rotating grid is to be correctly reproduced. In a flow without shear, rotation impedes spectral transfer of energy leading to higher energy levels than would otherwise be expected. We notice that Kim's large-eddy simulation does show higher levels of u' and v' compared with the stationary case in the central region of the channel where shear generation is negligible; the present computations do not, however, a result consistent with the findings of grid-

† Naot & Rodi (1982) have adopted a decay proportional to $(k^{\frac{1}{2}}/\epsilon y)^2$ to increase the fall-off rate.

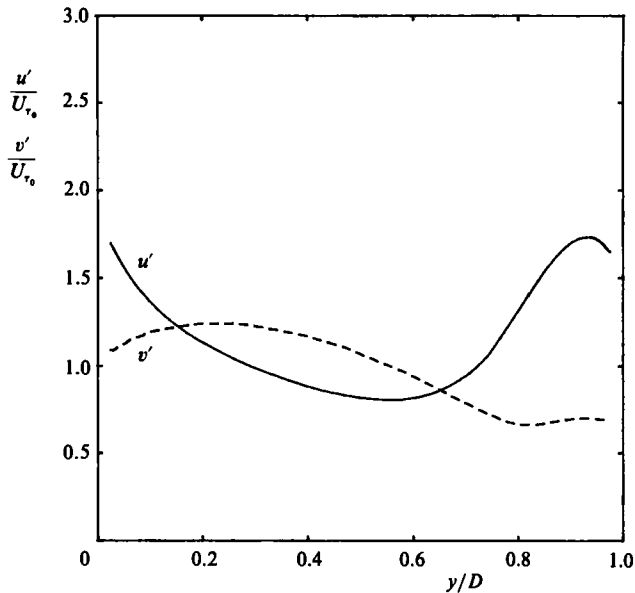


FIGURE 5. Computed turbulence intensity profiles for $Ro = 0.21$.

turbulence.† This weakness is of little significance in the present flow since its main characteristics are set by the regions closer to the wall where the predominant stress generation occurs.

Although experimental data are not available for comparison, it is of interest to note in figure 5 that for a Rossby number of 0.21 the augmentation of \bar{v}^2 and damping of \bar{u}^2 on the unstable side results in v' becoming greater than u' in the range $0.16 < y/D < 0.65$ (a result that qualitatively accords with the large-eddy simulation of Miyake & Kajishima 1986). Now, since $\bar{u}\bar{v}$ is negative in this region of the channel, the term $-2(\bar{u}^2 - \bar{v}^2)\Omega$ in the $\bar{u}\bar{v}$ equation now acts as a sink and this in turn acts to increase $\partial U/\partial y$ in this region. A steepening in velocity gradient is indeed the development observed in figure 2 at the highest Rossby number.

Finally, the effect of rotation on the wall friction coefficient is examined. Figure 6, adapted from Johnston *et al.* (1972), shows the variation with Rossby number of the friction velocity on each of the walls normalized by the friction velocity for zero rotation at the same Reynolds number. Even Rossby numbers of order 10^{-2} produce measurable differences in friction factor between the stable and unstable surfaces. On the unstable surface the augmentation appears to ‘saturate’ for $Ro \approx 0.07$ with U_τ some 10% higher than for the non-rotating case. The reason for the saturation is presumably that as \bar{v}^2 amplifies, the Coriolis source in the $\bar{u}\bar{v}$ equation is reduced (and, as discussed in the previous paragraph, eventually changes sign). In contrast, on the stable side \bar{v}^2 is diminished thereby increasing $(\bar{u}^2 - \bar{v}^2)$, so the sink in the $\bar{u}\bar{v}$ equation increases monotonically with Rossby number. There is consequently no tendency for U_τ/U_{τ_0} to reach an asymptotic value. The variations shown by the experimental results are mimicked by the present computations within the probable uncertainty of the data provided that the shear flow remains turbulent on both walls.

† Bardina *et al.* propose the inclusion of a rotational source in the ϵ equation, $-0.15\Omega\epsilon$, to mimic the experimental decay. In the present study the term was included for a single run at $Ro = 0.165$. The results generated were not significantly different from those with the standard ϵ equation.

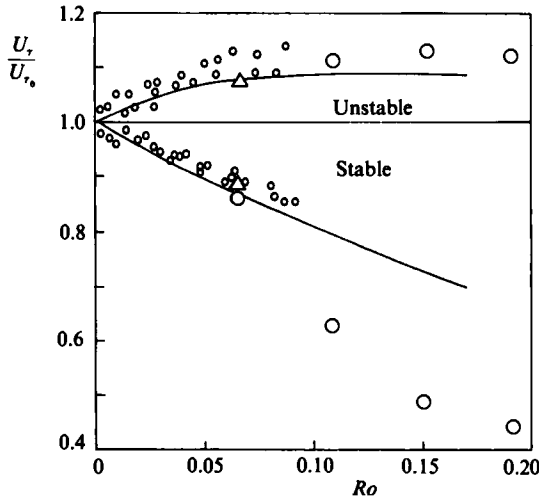


FIGURE 6. Effects of rotation on wall friction. $\circ\circ$, experimental data collected by Johnston *et al.* (1972); \triangle , large-eddy simulation by Kim (1983); \bigcirc , low-Reynolds-number data by Johnston *et al.* (1972); —, present predictions $Re = 35000$.

Experiments of Johnston *et al.* (1972) conducted at a Reynolds number of about 10^4 indicate that for Rossby numbers greater than about 0.1 the flow near the stable wall becomes laminar leading to a marked reduction in the level of friction factor there. This development is one that the calculations can obviously not reproduce since the wall boundary condition assumes a fully-turbulent layer in local equilibrium at the near-wall node.

4. Concluding remark

Our impression is that the second-moment closure in this study does capture the main effects of rotation on the turbulence structure. In particular, the fact that the further augmentation of shear stress at the unstable wall ceases beyond a Rossby number of about 0.07 is correctly accounted for. Moreover, the differing behaviour near the two walls has been traced to the fact that near the unstable wall the Coriolis source produces changes in $\overline{v^2}$ and $\overline{u^2}$ which progressively reduce the magnitude of the corresponding source in the \overline{wv} equation. The findings help support the view that the appearance of strikingly different large-scale structures in a shear flow does not necessarily signal a need to modify the turbulence model – at least if closure is made at second-moment level.

The work has been undertaken within a programme of research sponsored by Rolls-Royce plc. Authors' names appear alphabetically.

REFERENCES

- BARDINA, J., FERZIGER, J. H. & REYNOLDS, W. C. 1983 Improved turbulence models based on large-eddy simulation of homogeneous, incompressible, turbulent flows. *Mech. Eng. Dep. Rep. TF-19*, Stanford University.
- BARDINA, J., FERZIGER, J. H. & ROGALLO, R. S. 1985 *J. Fluid Mech.* **154**, 321.

- BERTOGLIO, J.-P. 1982 *AIAA J.* **20**, 1175.
- COLES, D. 1956 *J. Fluid Mech.* **1**, 191.
- COUSTEIX, J. & AUPOIX, B. 1981 *La Recherche Aéronautique*, no. 1981-4, p. 275.
- CROW, S. C. 1968 *J. Fluid Mech.* **33**, 1.
- DALY, B. J. & HARLOW, F. H. 1970 *Phys. Fluids* **13**, 2364.
- ERINGEN, A. C. 1962 *Non-Linear Theory of Continuous Media*, p. 93. McGraw Hill.
- GIBSON, M. M. & LAUNDER, B. E. 1978 *J. Fluid Mech.* **86**, 491.
- HANJALIĆ, K. & LAUNDER, B. E. 1972 *J. Fluid Mech.* **52**, 609.
- HOWARD, J. G. H., PATANKAR, S. V. & BORDYNUK, R. M. 1980 *Trans. ASME I: J. Fluids Engng* **102**, 456.
- JOHNSTON, J. P., HALLEEN, R. M. & LEZIUS, D. K. 1972 *J. Fluid Mech.* **56**, 533.
- KIM, J. 1983 *Proc. 4th Turbulent Shear Flows Symposium, Karlsruhe*, p. 6.14.
- KOYAMA, H. S. & OHUCHI, M. 1985 *Proc. 5th Turbulent Shear Flows Symposium, Cornell*, p. 21.19.
- LAUNDER, B. E. 1965 The effect of Coriolis force on fully-developed flow in a rotating duct. *MIT Gas Turbine Laboratory Rep.*
- LAUNDER, B. E., REECE, G. J. & RODI, W. 1975 *J. Fluid Mech.* **68**, 537.
- LESCHZINER, M. 1982 An introduction and guide to the computer code PASSABLE. *Mech. Eng. Dept. Rep. UMIST.*
- MASUDA, S., KOYAMA, H. S. & ARIGA, I. 1983 *Bull. JSME* **26**, 1534.
- MIYAKE, Y. & KAJISHIMA, T. 1986 *Bull. JSME* **29**, 1341.
- MOORE, J. 1967 *MIT Gas Turbine Lab. Rep.* 89.
- NAOT, D. & RODI, W. 1982 *J. Hydraul. Div. ASCE* **108**, 948.
- POUAGARE, M. & LAKSHMINARAYANA, B. 1983 *Proc. 4th Turbulent Shear Flow Symposium, Karlsruhe*, p. 6.6.
- ROTTA, J. 1951 *Z. Phys.* **129**, 547.
- SHIR, M. 1973 *J. Atmos. Sci.* **30**, 1327.
- TAKHAR, H. S. & THOMAS, T. G. 1985 Frame invariance of turbulence constitutive equations. Simon Engineering Laboratories, University of Manchester.